Preparation of controlled nanosized Ag particles by the DC arc plasma evaporation

XIAOMIN ZHANG, ZHENZHONG ZHANG*, FANGXIA ZHAO, TAI QIU, HAINING MENG
College of Materials Science and Engineering, Nanjing University of Technology, No. 5, Xin Mo Fan Road, Nanjing 210009, China

In order to prepare high-performance silver conductive paste, nanosized Ag particles were prepared by DC arc plasma reactor. The significant factors for the production rate and the particle size were researched by orthogonal experiments (OA_{16} matrix) and range analysis. The composition, structure and morphology of particles were investigated by X-Ray diffraction (XRD), transmission electron microscopy (TEM) and X-ray fluorescence (XRF), respectively. Silver particles were prepared by DC arc plasma, with a purity of up to 99.92 wt%, smooth surface and spherical form. The results show that the larger electric current can enhance the production rate and the average diameter. Both the particle size and the production rate increase as the P_{H2}/P_{Ar} increases. With the increase of pressure, the production rate decreases and the particle size rises first and then decreases.

(Received September 30, 2013; accepted January 22, 2014)

Keywords: DC arc plasma evaporation, Ag nanoparticles, Preparation, Average diameter, Production rate

1. Introduction

For their unique physical and chemical properties, Ag nanoparticles have been widely used as efficient catalysts [1], photonics [2], electrode materials [3]. They are especially efficient in conductive paste [4]. Many methods can be used to prepare Ag nanoparticles, such as Spray pyrolysis [5], electrolysis [6], microwave plasma method [7], mechanical synthesis [8], chemical reduction [9], magnetron plasmas [10] and DC arc thermal plasma method [11]. Because of low cost and high production rate, the DC arc plasma method has been successfully applied to manufacture Ni [12], Cu [13], Co [14] and Fe [15] nanoparticles. Through the method, spherical and controllable size of silver particles with high purity can be obtained. However, there exists no systematic study on the way of preparing silver with gas legal system. The factors affecting the Ag nanoparticles' production rate and particle size of the process have not been intensively investigated, which is important to obtaining particles with desired physical and chemical properties. High purity spherical silver powders with polycrystalline habit were obtained by optimizing growth conditions. Current, pressure and proportions of gas all have an effect on the production rate of silver and the average particle size, and their effect was investigated by orthogonal experiments. The coalescence growth mechanism of the Ag nanoparticles was also studied.

2. Experiment

2.1 Preparation

Fig. 1 shows the equipment of manufacturing silver nanoparticles by the DC arc plasma method. Silver bulk material was used as the raw material of manufacturing Ag nanoparticles by DC arc plasma evaporation method. Firstly, Ag bulk material was placed in a water-cooling crucible. Secondly, the preparation chamber was evacuated to 6×10^{-3} Pa by an external pumping system. Then the preparation chamber was filled with hydrogen and argon. The equipment in so preparation has the following advantages. The DC arc plasma equipment can not only improve the production rate but also manufacture metal powders with different particle sizes. Recycle gas and circulating cooling water system effectively increase energy utilization. Cyclone chamber with a low-pressure system can select powders and lead to a narrow size distribution.

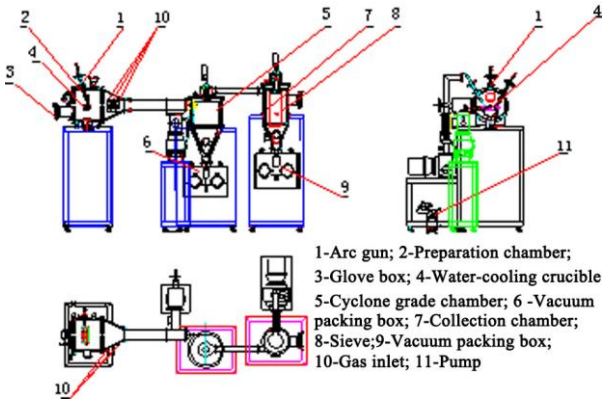

Fig. 1. Diagram of high vacuum three-gun DC arc plasma evaporation equipment for preparation of metal nanoparticles.

In the preparation stage, there are usually two ways

to generate evaporating atoms. One is through the interaction between two electrodes and metal surface. The interaction created a flux of evaporating atoms when the voltaic arc was ignited [16]. The other is through the heating of a metal surface [17]. As the metal vapor was oversaturated and collided with the argon gas around, a new stage was nucleated similarly from the aerosol systems [18-19]. Then some vapor was quickly cooled when colliding with water-cooling crucible and turned into primary particles by an aggregation growth mechanism [20]. Afterwards the metal particles were formed in the preparation chamber, and the fine particles can be separated from the primary particles thanks to the low-pressure of the cyclone classification system and the ultrafine particles can be obtained with controllable shape, narrow size distribution and high dispersivity. Generated ultrafine powders were blown into the cyclone grading chamber from the preparation chamber by the blower. Then the ultrafine powders were deposited on the collection chamber with the help of the cyclone airflow at room temperature under the protection of the high-purity gas. The particles were brought into the collection filter later, where the powders were deposited on the surface of the vessel's wall with high purity argon. Fine particles were scraped off inside the collection room by the scraper, and they fell into the vacuum collection box below. As the powders were collected in argon, silver powders did not aggregate. The particles prepared in this way had good dispersing properties and were not easily oxidized, because the high-purity hydrogen and argon adsorbed on the surface of the Ag particles.

During the preparation, the gas molecules were ionized into free electrons by the high voltage between the two electrodes, the phenomenon of ionization, in which the ionized molecules recombine with electrons or collide with one another. The energy released could melt the silver bulk materials to be metal melt. When the temperature was elevated to a certain extent, the kinetic energy of the metal atom was greater than its surface binding energy so that metal was melted to metal vapor. Then, when the metal vapor and argon collided, they rapidly spread from the center to the edge. In short, the current had an impact on the arc energy. As a result, the inflating pressure influenced the nucleation process of the mean free path. And hydrogen affected the metal evaporation rate. For these reasons, the orthogonal experiment should consider the impact of current, inflating pressure and P_{H2}/P_{Ar} ratio on particle sizes and production rate.

Therefore, the experiments were performed with sixteen well-planned orthogonal arrays (OA_{16} matrix). The three factors of current, pressure, and hydrogen-argon ratio which affect the production rate of and the average particle size were investigated. Each of these parameters was of four different levels. The current intensity is set at 200 A, 280 A, 360 A and 440 A, respectively; the filling pressure is set at 0.02 MPa, 0.04 MPa, 0.06 MPa and 0.08 MPa and the P_{H2}/P_{Ar} ratio at 1/6, 1/3, 2/3 and 1.

2.2. Characterization

The structure and the composition of the particles were analyzed by XRD and XRF, respectively. TEM was used to visualize the size and shape of the resulting nanoparticles [21-22]. The software of Simple PCI (US, Compix Company) was applied to calculate the average diameter with multiple images of TEM. Selected-area electron diffraction (SAED) was used to observe the polycrystalline structure.

3. Results and discussion

3.1 Structure and morphology

Fig. 2 shows the XRD pattern of the Ag particles with average particle size of 54 nm. Ag particles were produced via DC arc plasma evaporation method (the filling pressure is 0.04MPa, the P_{H2}/P_{Ar} ratio 2/3, the current 440A). All these peaks can be indexed based on cubic structure (Fm3m, JCPDF, No.04-0783) without any impure phases as shown in Fig. 2. According to the diffraction peak positions, it can be known that the unit cell parameters are a=b=c=4.0828nm. Compared with the standard card (04-0783), there is a slight contraction of the cell parameters and the cell volume is reduced by 0.057%. A possible reason is that the surface tension increases with the decrease of particle size. The surface tension can make lattice shrink obviously, and the lattice contraction is intensified. The nanoparticles analyzed by XRF show that Ag content is about 99.92 wt% and the main impure elements may come from the device. In general, the prepared particles are still of relatively high purity.

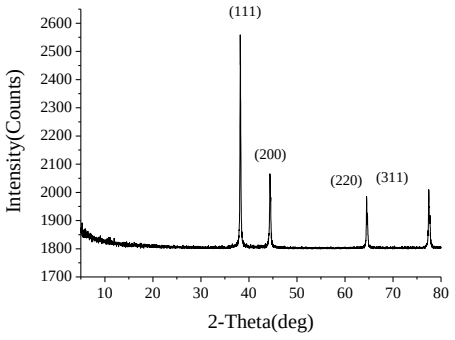

Fig. 2. XRD pattern of the Ag particles with average particle size of 54 nm.

Fig. 3, including (a) and (b), shows TEM images of a typical sample of Ag particles and indicates that the spherical morphology and smooth surface are achieved by this approach. Fig. 3 (b) shows the high magnification TEM image of Ag particles. The continuous electron diffraction pattern of the primary particle is illustrated in

Fig. 3 (c).

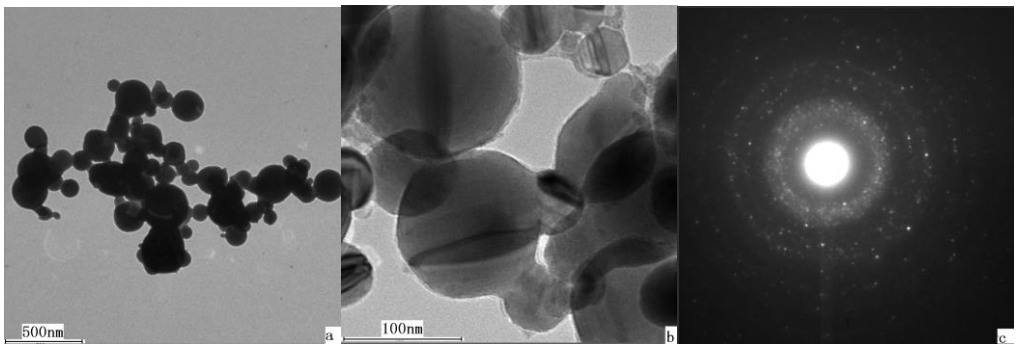

Fig. 3. TEM images of silver particles ((a) low magnification and (b) high magnification) and electron diffraction patterns (c).

The diffraction rings of commutative brightness and darkness imply excellent crystallinity of internal polycrystalline structure. The tropism of the particles in a random manner and small particles results in the widening of diffraction rings which contain a number of the diffraction spots. Apart from a few big light spots, it is shown in the figure that the diffraction rings are still consistent. The result demonstrates that spherical nano-polycrystalline primary particles form immediately by agglomeration of nucleus crystalline during evaporation-condensation.

3.2 Effect of electric current, P_{H2}/P_{Ar} ratio and gas pressure on the production rate and particle size

In the orthogonal experiments, 16 different groups of conditions were considered. Table1 shows the orthogonal experiments and the results. Based on the analysis of the data, the average diameter of the controlled nanosized particles ranged from 39 to 221nm by changing the process parameters. The letters A, B, and C represent the filling pressure, P_{H2}/P_{Ar} ratio, and current, respectively. X stands for the value of this experiment. Optimal production conditions (maximize production rate and suitable particle size) can be obtained by the orthogonal experiments.

Table 1. The orthogonal layout design and the results of the $L_{16}(4^3)$ orthogonal experiments.

No.	Filling Pressure (A/MPa)	P_{H2}/P_{Ar} ratio(B)	Current(C/A)	Productive efficiency($g \cdot h^{-1}$)	Average Diameter(nm)
1	0.02	1/6	200	6	39
2	0.02	1/3	280	209	42
3	0.02	2/3	360	679	175
4	0.02	1/1	440	1211	221
5	0.04	1/6	280	71	103
6	0.04	1/3	200	21	117
7	0.04	2/3	440	978	54
8	0.04	1/1	360	891	129
9	0.06	1/6	360	446	125
10	0.06	1/3	440	935	148
11	0.06	2/3	200	63	139
12	0.06	1/1	280	588	195
13	0.08	1/6	440	701	204
14	0.08	1/3	360	562	177
15	0.08	2/3	280	299	120
16	0.08	1/1	200	63	153

Table 2 shows the range analysis of the orthogonal experiments. Corresponding to the same level, $\overline{K_1}$, $\overline{K_2}$, $\overline{K_3}$, $\overline{K_4}$ were average experimental values of different factors. At the same level, R shows the maximum and minimum differences in values of $\overline{K_1}$, $\overline{K_2}$, $\overline{K_3}$, $\overline{K_4}$. The larger the corresponding R is, the more effect Ag particles have on the average diameter and the production rate.

Table 2. Range analysis of the $L_{16}(4^3)$ orthogonal experiments.

	Productive Efficiency(g/h)			Average Diameter/nm		
No.	Filling Pressure (MPa)	P_{H2}/P_{Ar} ratio	Current(A)	Filling Pressure (MPa)	P_{H2}/P_{Ar} ratio	Current(A)
Ⅰ	526	306	38	119	118	112
Ⅱ	490	418	233	101	121	115
Ⅲ	447	505	644	152	122	151
Ⅳ	406	630	954	164	175	157
R	120	324	916	63	57	45

Two important parameters (K_{ji}, R_j) are used to explain Table2. K_{ji} represents the sum of the evaluation indexes of all levels $(i, i=1,2,3,4)$ in each factor $(j, j=A,B,C)$. $\overline{K_{ji}}$ (average of K_{ji}) determines the optimal level and the optimal combination of the factors. The optimal level of each factor is obtained when the values of $\overline{K_{ji}}$ are at their peaks. Rj stands for the range between the maximum and the minimum values of $\overline{K_{ji}}$. It is used to evaluate the weights of the factors. This means that a larger R_j value shows a greater importance of the factor [23]. For instance, the calculation of K_{ji} and R_j is shown as the following formula. The K values of the factor A （Filling Pressure）can be calculated as follows:

$$\overline{K_{A1}} = \frac{K_{A1}}{4} = \frac{X_1 + X_2 + X_3 + X_4}{4} \quad (1)$$

$$\overline{K_{A2}} = \frac{K_{A2}}{4} = \frac{X_5 + X_6 + X_7 + X_8}{4} \quad (2)$$

$$\overline{K_{A3}} = \frac{K_{A3}}{4} = \frac{X_9 + X_{10} + X_{11} + X_{12}}{4} \quad (3)$$

$$\overline{K_{A4}} = \frac{K_{A4}}{4} = \frac{X_{13} + X_{14} + X_{15} + X_{16}}{4} \quad (4)$$

$$R_j = \max(\overline{K_{Ai}}) - \min(\overline{K_{Ai}}) \quad (5)$$

Where K_{Ai} is the K value of the i level of the factor A; X_i is the value of the result of the table 1 No. i. The other values of K are determined following the same calculation procedures. The results show that the effects of the conditions on average particle size have the following pattern (from strong to weak): filling pressure, P_{H2}/P_{Ar} ratio, and electric current. The effects of the conditions on the production rate have the following pattern (from strong to weak): electric current, P_{H2}/P_{Ar} ratio, filling pressure. The electric current is a key factor to the production rate, and the gas pressure also is a key factor to the particle size.

The controllable size Ag particles can be prepared by the DC arc plasma evaporation. The average particle size varies from 39 to 221 nm and the production rate ranges from 6 to 1211 g/h with different technical parameters. Fig. 4 shows the typical TEM images (a, b, c, d) by orthogonal experiments. The average particle sizes are 39, 54, 103, and 177nm, respectively. The prepared Ag particles have

some agglomeration. Before use, surfactants can be applied to coat them with ultrasound, giving them good dispersivity. The treated particles exhibit excellent performance in the conductive paste.

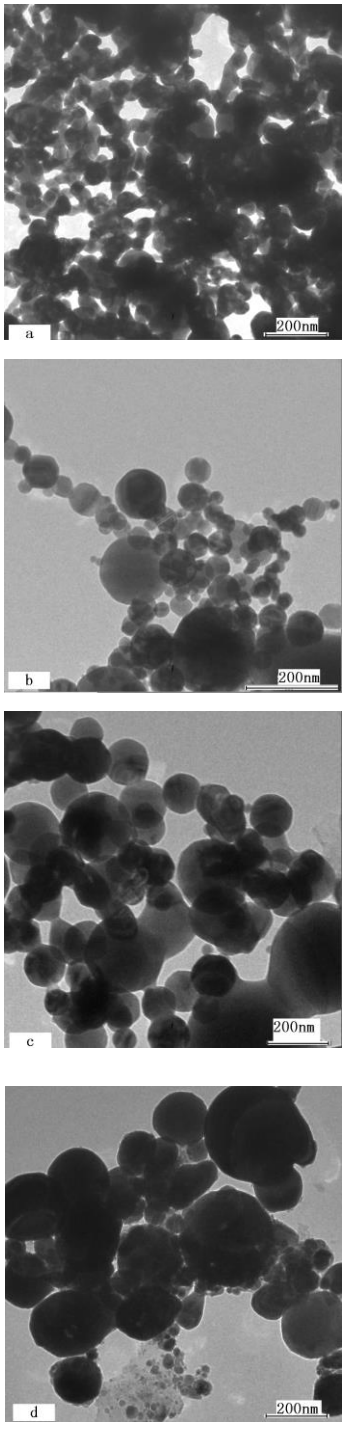

Fig. 4. Typical TEM images of silver nanoparticles under different conditions. (a)Filling Pressure 0.02 MP, P_{H2}/P_{Ar} ratio 1/6, Current 200 A; (b) Filling Pressure 0.04 MP, P_{H2}/P_{Ar} ratio 2/3, Current 440 A; (c) Filling Pressure 0.04 MP, P_{H2}/P_{Ar} ratio 1/6, Current 280 A; (d) Filling Pressure 0.08 MP, P_{H2}/P_{Ar} ratio 1/3, Current 360 A.

3.2.1 The effects of electric current on the production rate and the average particle size

Fig. 5 shows the effects of electric current on the production rate and the particle size of the prepared Ag particles with the same values of the filling pressure and P_{H2}/P_{Ar}. Table 2 lists the corresponding values of different factors on the particle size and production rate at the same level. As shown in Fig. 5, electric current significantly affects the production rate and the particle size of the particles, both of which increase with the increase of the electric current. When the current reaches 440 A, the average particle size of Ag nanoparticles reaches a peak of 157 nm, and the average particle size increases by about 40%. When the current rises from 200 to 440 A, the production rate increases from 38 to 954 g/h.

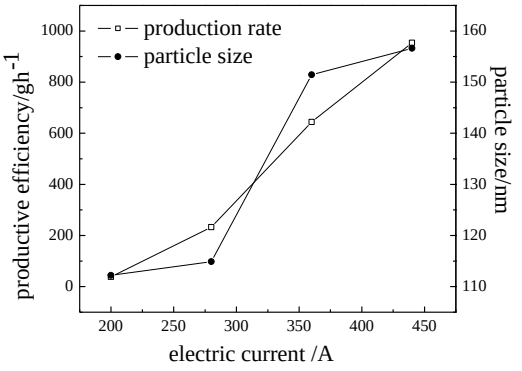

Fig. 5. Effect of electric current on the production rate and particle size of Ag nanoparticles.

During the evaporation, the relationship between the entire absorbed heat (Q_a) and the production rate (η) can be generally demonstrated by Eq. (6). In this experiment, the apparatus provides effective energy (Q_p) in Eq. (7). The absorbed energy (Q_a) is equal to the provided effective energy (Q_p). Therefore, Eqs. (6) and (7) can be rearranged as Eq. (8). When the voltage keeps constant during the preparation of Ag particles, stronger electric current can provide higher energy, which increases the production rate (η) of the particles.

$$Q_a = (K + C_3T_2)\,m = 60\,\eta\tau(K + C_3T_2) \quad (6)$$

$$Q_p = aIU\tau \quad (7)$$

$$\eta = \frac{aIU}{60(K + C_3T_2)} \quad (8)$$

Where T_2 is the temperature of metallic vapor, C_3 (J/g·k) is the specific heat between T_2 and melting point, τ (min) is the evaporation time, K, a are constants, I is the electric current, U is the voltage.

In the process of evaporation-condensation, the stage transforms from the oversaturated vapor to the nanoparticles by homogeneous nucleation mechanism which is followed by growth through condensation and coagulation. The formation and growth of nanoparticles can be described as a Brown coagulation [24]. With sharp-cooling, the Ag vapor directly changes into solid particles. The particle growth can be confined without affecting the nucleation rate. On the basis of the nucleation thermodynamics, the particle size of the products depends on the ratio between the nucleation rate and growth rate. In the study, the particle size can be formulated as equation (9) [25]

$$D = \sqrt[3]{\frac{6C_0M}{\pi N\rho}} \tag{9}$$

Where M (g /mol) is the quality of the atom, C_0 (mol/ml) is the concentration of the vapor, N (ML^{-1}) is the particle number per unit volume, ρ (g/cm^3) is the particle density.

Eq. (9) shows that the particle size has the direct ratio to the cubic root of the metal vapor concentration C_0 but is reciprocal to the cubic root of the particle number per unit volume N. It can be seen that a stronger electric current results in higher concentrations of vapor, more particles per unit volume, and more collisions between particles. In this narrow region, the further growth of the particles occurs mainly by coalescence to form larger particles, which leads to the decrease of value N and increase of value D. In other words, the particle diameter increases.

3.2.2 The effect of P_{H2}/P_{Ar} ratio on the production rate and the average particle size

Fig. 6 shows the effect of the P_{H2}/P_{Ar} ratio on the production rate and the particle size of Ag particles with the same values of the filling pressure and the current. The values of the average diameter and production rate correspond, under the same P_{H2}/P_{Ar} ratio, to those in Table 2.

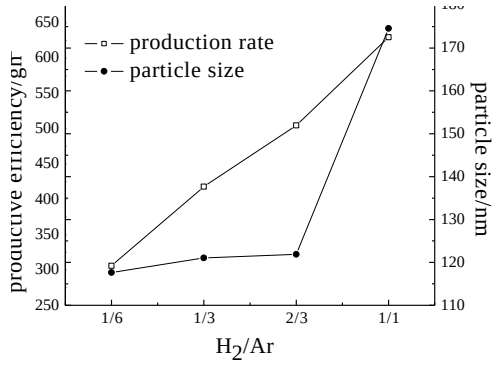

Fig. 6. Effect of P_{H2}/P_{Ar} ratio on the production rate and particle size of Ag nanoparticles.

The result indicates that the production rate and particle size increase as the value of the P_{H2}/P_{Ar} ratio increases. Fig. 6 shows that the average diameter increases with the increase of the P_{H2}/P_{Ar} ratio, and the average diameter increases by 48%, from 118 to 175 nm. When the P_{H2}/P_{Ar} ratio increases from 1/6 to 1, the production rate increases by 106%, from 306 to 630 g/h.

Different results were obtained when the device was filled with a mixture of hydrogen and argon and with only argon. In the former case, after the first half of the experiment, the remaining metal bulk was taken for wire cutting and many stomata were found on the cut surface. However, no stomata were found in the latter case.

Hydrogen atoms (H) are generated by high-temperature decomposition of H_2 gas. Hydrogen atoms continuously go into the molten metal. The concentration of active hydrogen atoms is greater than the maximum solubility in the metal. Meanwhile, a lot of hydrogen atoms reconstruct to the form of hydrogen molecules , which enlarges the high-temperature zone contributing to the acceleration of the evaporation. When the energy is released, the hydrogen molecules form bubbles in the molten metal. They enter into the metal, and flow away from the molten metal with metal vapor. Finally, when the pressure within the bubbles reaches the critical value, the bubbles burst, and the metal vapor is rapidly cooled. The initial Ag particles are formed by aggregation-growth mechanism. When P_{H2}/P_{Ar} ratio reaches 1/1, the metal melt begins to boil with the swashing melts when a large number of hydrogen gas bubbles escape from the center of the metal melts. Therefore, the addition of hydrogen has changed the evaporation model to be the boiling evaporation with a greater evaporation rate. Thus, the larger P_{H2}/P_{Ar} ratio provides stronger energy and improves the production rate of the particles, which lead to an increase in the particle diameter.

3.2.3 The effect of the filling pressure on the production rate and the average particle size

Fig. 7 shows the effect of the filling pressure on the production rate and particle size with the same values of P_{H2}/P_{Ar} and the current. The outcomes of both the average diameter and the production rate are the values under the same gas pressure of the same matching level in Table 2. The production rate decreases as the gas pressure increases (Fig. 7). However, the particle size presents an interesting phenomenon and the smallest particle can be obtained when gas pressure is equal to 0.04 Mpa. When the gas pressure rises from 0.04 to 0.08 Mpa, the average diameter increases by 62%, from 101 to 164 nm. The production rate, however, decreases from 526 to 406 g/h.

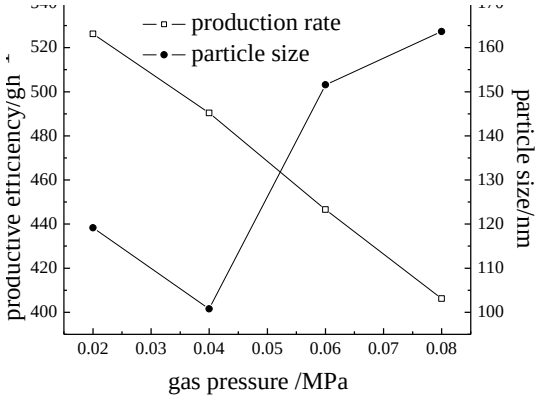

Fig. 7. Effect of gas pressure on the production rate and particle size of Ag nanoparticles.

The production rate decreases with the increase of the filling gas pressure. It can be assumed that when the gas pressure increases, the evaporated atoms collide with each other and fall back to the melting metal. Then the decrease of the vapor concentration leads to decrease in particle size and production rate. It is mainly attributed to the influence of the pressure on the average free path. From available literature [25], the average free path depends on the pressure and its relationship can be declared as (10). Therefore, the increase of the p leads to the decrease of the value $\overline{\lambda}$ and increase of the collision frequency. Then, further growth of particles occurs mainly by coalescence leading to larger particle sizes. It is also shown that there are some argon molecules on the evaporating surface of the metal when the gas pressure is low. Thus, the crystal nucleus of the silver meets very small obstacles from argon molecules, and the silver particles can quickly escape from the liquid surface. Because of adsorption vapor, the nucleus of Ag is not able to grow further, which leads to a small average diameter. When the pressure increases, the grain diameter increases as well.

$$p\overline{\lambda} = k \tag{10}$$

Where p is the gas pressure, $\overline{\lambda}$ is the mean free path, k is a constant.

4. Conclusions

Spherical silver particles were produced by DC arc plasma with a purity of up to 99wt% and smooth surface. The silver nanoparticles present a cubic crystal structure with a slight lattice contraction. The average diameter of the controlled nanosized particles ranges from 39 to 221 nm by changing the processing parameters. The experiments show that stronger electric current results in an increase in the production rate and the size of the particles. The particle size and the production rate rise with the P_{H2}/P_{Ar} ratio. The production rate decreases with the increase of the filling gas pressure.The particle size rises first and then decreases. The electric current is the key factor to the production rate, and the gas pressure is the key factor to the particle size. The effects of the conditions on the average particle size have the sequence (from strong to weak): filling pressure, P_{H2}/P_{Ar} ratio, electric current. The effects of the conditions on production rate have the following pattern (from strong to weak): electric current, P_{H2}/P_{Ar} ratio, filling pressure.

Acknowledgements

A Project Funded by the Priority Academic Program Development of Jiangsu Higher Education Institutions.

References

[1] M. N. Chen, D. Y. Zhang, L. T. Thompson, Z. F. Ma, International Journal of Hydrogen Energy, **36**, 7516 (2011).
[2] R. K. Gupta, K. Ghosh, R. Patela, P. K. Kahol, Optoelectron. Adv. Mater.- Rapid Comm. **12**(2), 792 (2008).
[3] L. Chu, X. L. Zhang, Journal of Electroanalytical Chemistry, **665**, 26 (2012).
[4] G. G. Umarji, S. A. Ketkar, G. J. Phatak, V. D. Giramkar, U. P. Mulik, D. P. Amalnerkar, Microelectronics Reliability, **45**, 1903 (2005).
[5] Y. N. Ko, S. H. Choi, Y. C. Kang, Journal of the European Ceramic Society, **33**, 1335 (2013).
[6] M. Z. Kang, Y. P. Liu, R. M. Si, Applied Surface Science, **258**, 5533 (2012).
[7] T. H. Nguyen, K. H. Lee, B. T. Lee, Materials Science and Engineering: C, **30**, 944 (2010).
[8] G. R. Khayati, K. Janghorban, Advanced Powder Technology, **23**, 393 (2012).
[9] K. D. Bhatte, K. M. Deshmukh, Y. P. Patil, D. N. Sawant, S. I. Fujita, M. Arai, B. M, Particuology, **10**, 140 (2012).
[10] J. Li, Y. Fang, Spectrochimica Acta Part A: Molecular and Biomolecular Spectroscopy, **66**, 994 (2007).
[11] S. H. Lee, S. M. Oh, D. W. Park, Materials Science and Engineering: C, **27**, 1286 (2007).
[12] Z. Q. Wei, T. D. Xia, L. F. Bai, J. Wang, Z. G. Wu, P. X. Yan, Materials Letters, **60**, 766 (2006).
[13] Z. Q. Wei, T. D. Xia, J. Ma, W. J. Feng, J. F. Dai, Q. Wang, P. X. Yan, Transactions of Nonferrous Metals Society of China, **17**, 128 (2007).
[14] H. N. Meng, F. X. Zhao, Z. Z. Zhang, International Journal of Refractory Metals and Hard Materials, **31**, 224 (2012).
[15] J. Noma, H. Abe, T. Kikuchi, J. Furusho, M. Naito, Journal of Magnetism and Magnetic Materials, **322**, 1868 (2010).

[16] B. M. Smirnov, Contributions to Plasma Physics, **44**, 558 (2004).
[17] B. M. Smirnov, I. Shyjumon, R. Hippler, Physica Scripta, **73**, 288 (2006).
[18] J. H. Scott, S. A. Majetich, Physical Review B, **52**, 12564 (1995).
[19] B. M. Smirnov, Physica Scripta, **64**, 152 (2001).
[20] Z. L. Wang, Y. Liu, Z. Zhang, Beijing, (2002).
[21] A. A. Ashkarran, Current Applied Physics, **10**, 1442 (2010).
[22] A. H. Li, Y. W. Wang, Q. Q. Yu, Rare Metal Materials and Engineering, **38**, 327 (2009).
[23] C. W. Cui, F. Shi, Y. G. Li, S. Y. Wang, Journal of Materials Science: Materials in Electronics, **21**, 349 (2010).
[24] S. Kasukabe, Journal of Crystal Growth, (196-200), 99 (1990).
[25] Y. H. Qin, High Education Press, Beijing, (2011).

*Corresponding author: zhangxiaominnjut@126.com